Aalto University

Aaltodoc

OPEN ACCESS

Author(s):   Kujala, J. & Segercrantz, N. & Tuomisto, Filip & Slotte, J.

Title: Native point defects in GaSb

Year: 2014

Version: Final published version

Native point defects in GaSb

J. Kujala, N. Segercrantz, F. Tuomisto, and J. Slotte

Articles you may be interested in

Publisher's Note: "Point defect balance in epitaxial GaSb" [Appl. Phys. Lett. 105, 082113 (2014)]
Appl. Phys. Lett. **105**, 169901 (2014); 10.1063/1.4896700

Point defect balance in epitaxial GaSb
Appl. Phys. Lett. **105**, 082113 (2014); 10.1063/1.4894473

Antisites and anisotropic diffusion in GaAs and GaSb
Appl. Phys. Lett. **103**, 142107 (2013); 10.1063/1.4824126

Influence of substrate doping and point defects on Al and Ga interdiffusion in AlSb/GaSb superlattice structures
J. Appl. Phys. **102**, 023511 (2007); 10.1063/1.2743883

Native defects and self-diffusion in GaSb
J. Appl. Phys. **91**, 4988 (2002); 10.1063/1.1462844

Native point defects in GaSb

J. Kujala, N. Segercrantz, F. Tuomisto, and J. Slotte
Department of Applied Physics, Aalto University School of Science, P.O. Box 14100, FI-00076 AALTO, Finland

We have applied positron annihilation spectroscopy to study native point defects in Te-doped *n*-type and nominally undoped *p*-type GaSb single crystals. The results show that the dominant vacancy defect trapping positrons in bulk GaSb is the gallium monovacancy. The temperature dependence of the average positron lifetime in both *p*- and *n*-type GaSb indicates that negative ion type defects with no associated open volume compete with the Ga vacancies. Based on comparison with theoretical predictions, these negative ions are identified as Ga antisites. The concentrations of these negatively charged defects exceed the Ga vacancy concentrations nearly by an order of magnitude. We conclude that the Ga antisite is the native defect responsible for *p*-type conductivity in GaSb single crystals. © *2014 AIP Publishing LLC*. [http://dx.doi.org/10.1063/1.4898082]

I. INTRODUCTION

The material properties of gallium antimonide (GaSb) allow it to be used in various optical and electrical applications.[1–3] This material belongs to the III-V family of compound semiconductors, and has a lattice constant of 6.0959 Å.[4] In solid state, it has the zincblende structure. GaSb also has a relatively narrow band gap of 0.725 (0.822) eV at 300 K (0 K).[4] Such a gap is beneficial when fabricating, e.g., infrared detectors. With high electron mobility and high saturation velocity,[5] it is a good choice for high electron mobility transistors. GaSb based structures can also be used, for example, in laser diodes, in booster cells, in tandem solar cell arrangements, and in high efficiency thermophotovoltaic cells.[4] Recently, significant attention has been given to the lattice properties of GaSb when dopant atoms are introduced into the lattice during the growth phase.[6–9]

Surprisingly few experimental studies on the defect properties of GaSb can be found. Intrinsic defects and defect complexes can introduce energy levels in the forbidden band gap, which can act as compensating centers or charge carrier traps. This can have a detrimental influence on the electrical properties of semiconductor devices. Bracht *et al.*[10] studied self-diffusion properties of gallium and antimony in the GaSb sublattices. They noted that Ga and Sb atoms diffuse in GaSb isotope heterostructures independently in their own sublattices. Under Ga-rich conditions, V_{Sb} is unstable and cannot take part in Sb self-diffusion. On the other hand, Ga vacancies are formed easily and contribute to Ga self-diffusion in the Ga sublattice. Under Sb-rich conditions, gallium vacancies and Sb interstitials undergo a transformation yielding Sb-antisites. This correspondingly results in a low concentration of Sb-interstitials and inefficient Sb diffusion.

Deep donor levels (DX-centers) are known to be important defects controlling the conductivity in some of the III-V compounds.[11,12] Poole *et al.*[13] reported a deep state also in moderately sulfur doped GaSb. According to this study, the defect responsible for the deep state has similar properties as the DX center in AlGaAs systems. Interestingly, they found

a similar defect level in GaSb doped with tellurium. Du and Zhang[12] studied the presence of the DX center in GaAs and GaSb using density functional theory (DFT) within the local density approximation. In this study, they find a DX center with double donor defect structure with its stability strongly dependent on the size of the dopant atom.

Undoped GaSb is *p*-type independent of the applied growth method,[4] but the origin of the *p*-type conductivity is still under debate. Theoretical calculations have been employed to shed light on this issue. Most recently, Virkkala *et al.*[14] studied GaSb by using the DFT framework with hybrid functionals. They reported that the Ga_{Sb}^{2-} formation energy was relatively low in Ga rich growth conditions. This defect was suggested to be the reason for *p*-type conductivity. Furthermore, it was noted that the formation energy of Sb_{Ga} was also quite low in Sb-rich growth conditions. The Sb antisite works effectively as a donor in GaSb and contributes to *n*-type conductivity and has a compensating effect on *p*-type conductivity.

Positron annihilation spectroscopy (PAS) is well suited for studying point defects in solids, with selective sensitivity to negative and neutral vacancy defects and negatively charged defects without open volume.[15] Positron methods are insensitive to the electrical conductivity of the material and can be easily applied both to metals and semiconductors regardless of the width of the band-gap. The identification of mono- and di-vacancy defects in Ge provides a good example in narrow band gap semiconductors.[16,17] Furthermore, positron methods are well supported by theory and the annihilation characteristics can be calculated from first principles.

Positron studies have been performed also earlier in GaSb. Ling *et al.*[18] studied undoped as-grown and electron irradiated GaSb samples with positron and Hall measurement techniques. They reported an acceptor level that was suggested to be related to the Ga antisite. This antisite defect was suggested to be responsible for *p*-type conductivity in GaSb. Similarly Hu *et al.*[19] studied undoped GaSb samples. They observed a 288 ps lifetime component that they associated with the positron lifetime in a Ga vacancy. Hu *et al.* suggested that V_{Ga} related defects are the dominating

vacancy defects in undoped GaSb samples. These vacancies were observed to anneal out at 520 °C.

In this work, we have applied positron annihilation spectroscopy to study native point defects and to identify the origin of *p*-type conductivity in bulk GaSb. Both positron lifetime and Doppler broadening measurements were performed as a function of temperature. We conclude that Ga vacancies indeed are the dominant vacancy defects observed with positrons, but Ga antisites in negative charge state are an order of magnitude more abundant and dominate the positron annihilation signal. Hence, Ga antisites cause the *p*-type conductivity in bulk GaSb.

II. EXPERIMENTAL DETAILS

We have studied Czochralski grown tellurium doped *n*-type ([Te] $\approx$ 6×10^{17} cm^{-3}, [n] $\approx$ 1.6×10^{17} cm^{-3}, $\mu_{Hall} \approx 5200 \frac{cm^2}{V \cdot s}$) and unintentionally *p*-type GaSb ([p] $\approx$ 1.3×10^{17} cm^{-3}, $\mu_{Hall} \approx 700 \frac{cm^2}{V \cdot s}$) (hereafter, referred to as *n*- and *p*-type GaSb, respectively) with positron lifetime- and Doppler broadening spectroscopies. The samples were provided by Wafer Technology Ltd. (Tongwell, United Kingdom).

For the positron lifetime measurements, the standard sandwich setup was used, where a ^{22}Na e$^+$-source is sandwiched between two identical samples. The sample package was placed in a closed cycle helium cryostat equipped with resistive heating elements and a sapphire thermal interface. The measurements were performed in vacuum at temperatures 30–580 K.

After implantation into the sample, positrons thermalize and diffuse, ultimately annihilating with electrons. Annihilation with electrons occurs while the positron is either in a delocalized state in the lattice or trapped at a defect. In the annihilation event, two gamma quanta are emitted with an energy of 511 keV. The positron lifetime is the time difference between one of these two 511 keV photons and the 1.27 MeV photon emitted together with the positron in the β-decay of ^{22}Na. Typically, $\sim 10^6$ annihilation events are collected into a positron lifetime spectrum.

A conventional coincidence Doppler broadening setup was used. The HPGe detector resolution was 1.34 keV at 511 keV. In this method, the HPGe detector is used to measure the Doppler broadening of the 511 keV annihilation line, and another detector is used as a coincidence gate. With this setup, the peak-to-background ratio was 10^4. The Doppler measurements we performed using a monoenergetic e$^+$ beam with acceleration voltage of 35 kV. Approximately 10^6 counts were collected for each spectrum.

Trapping of positrons at vacancies is seen as an increase in the positron lifetime due to the locally reduced electron density at the annihilation site of the positron. This also leads to the narrowing of the Doppler broadened spectrum of the 511 keV annihilation lines, as the probability of positron annihilation with high-momentum core electrons is reduced. Negatively charged non-open volume defects, such as acceptor impurities, can trap positrons at shallow Rydberg-like states, but the annihilation signals are the same as for the defect-free lattice due to the wide spatial extent of the Rydberg states. The trapping efficiency of negatively

charged defects (both vacancies and ions) increases at low temperatures, while neutral vacancy defects exhibit no temperature dependence.

III. RESULTS

A. Lifetime measurements

Figure 1 shows lifetime spectra from the *n*- and *p*-type samples at different temperatures. The positron lifetime spectrum is a sum of exponentially decaying components of the form $\exp^{-\lambda_i t}$, where $\lambda_i (= \tau_i^{-1})$ is the positron annihilation rate in state i and *t* is the measured time. If the sample has no detectable amount of vacancies, the spectrum has a single exponential component, hence showing linear behavior on log scale. Each slope in the tail part of the spectra corresponds to an annihilation state, which has its own intensity and lifetime. Decomposition of the spectrum into several components is usually successful only if the lifetime components are well separated, i.e., $\frac{\tau_{i+1}}{\tau_i} > 1.3 - 1.5$.[15] Typically, at most three lifetime components can be resolved reliably from a lifetime spectrum.

In the present case, two components could be fitted to the experimental lifetime data. The simplest interpretation then follows a two-component trapping model, where only one type of defect is trapping positrons. The average positron lifetime is expressed in the following form:

$$\tau_{ave} = I_1 \tau_1 + I_2 \tau_2. \quad (1)$$

The average lifetime is the superposition of two states; τ_1 and τ_2 describe the positron lifetime in the lattice (reduced
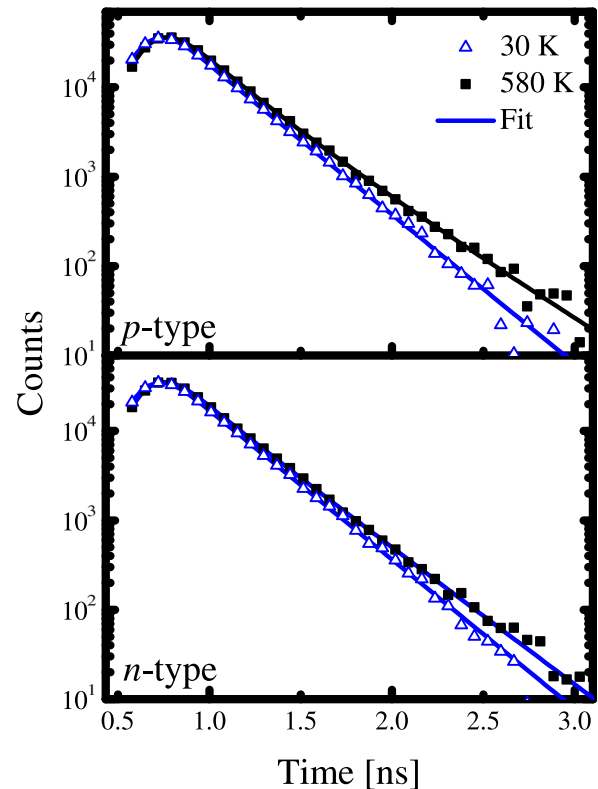

FIG. 1. Lifetime spectra of *n*- and *p*-type GaSb measured at different temperatures. The fit of the two-component model is shown as a solid line.

lifetime) and in the defect, respectively. The coefficients I_i are the intensities of each lifetime component τ_i in the spectrum. Within the context of the two-component model, an increase in τ_2 is an indication of bigger defect size and larger open volume and a higher I_2 signals an increase in the defect concentration.

Figure 2 shows decompositions of the lifetime spectra. The samples were measured in series from 30 K to 580 K and back to 30 K. Two lifetime components were decomposed from the *n*- and *p*-type GaSb lifetime spectra, respectively. The two-component model seems to give reasonable results when fitted to *n*-type spectra measured above 330 K, where $I_2 \sim 90\%$ and τ_2 evens out with $\tau_2 = 280 \pm 5$ ps. This type of a lifetime corresponds to a positron lifetime in a monovacancy size defect, where the positron lifetime is typically 10%–20% higher compared to the defect free lattice. It should be noted that τ_2 changes strongly and I_2 approaches
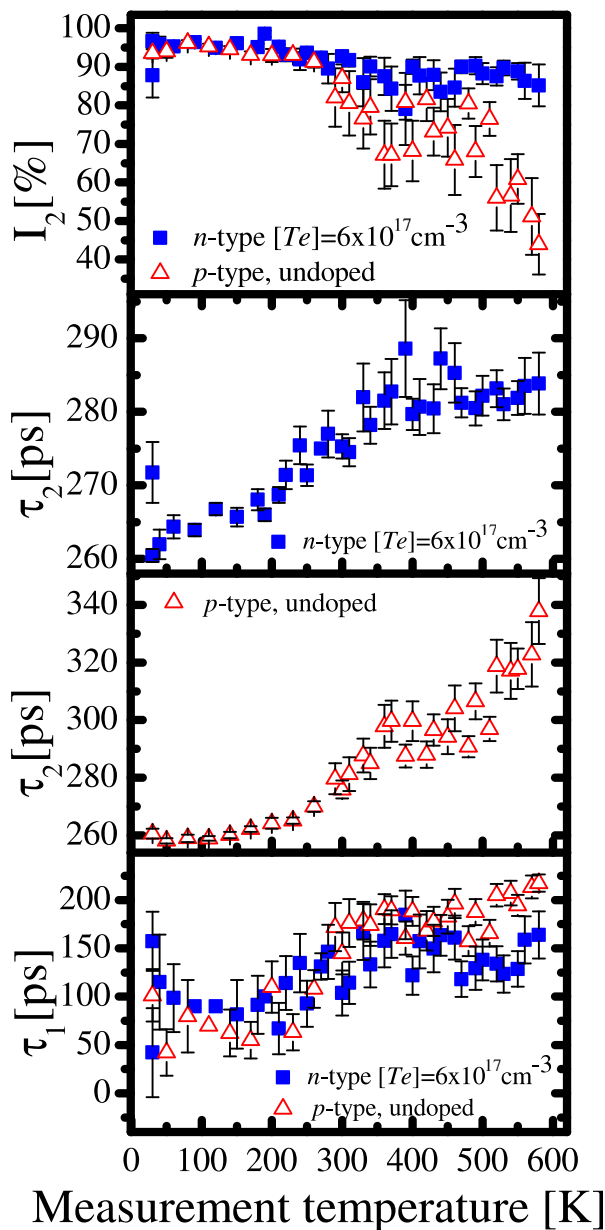
100% below 330 K. This indicates that the two-component model is insufficient to fully describe the data, meaning that more than one positron trap are actively trapping positrons in the sample. However, as fitting more than two components to the lifetime was unsuccessful, likely due to the mutual closeness of the lifetime components, we apply the two-component model for analysis. The consequences of having more than one positron trap are taken into account in the following discussion. In *p*-type, GaSb a plateau is observed in the temperature range 360–510 K, where τ_2 evens out with $\tau_2 = 295 \pm 10$ ps. This plateau probably corresponds to the same monovacancy defect as is observed in *n*-type GaSb. Also here the two-component trapping model is insufficient below 350 K. The increase of τ_2 (and decrease of I_2) at temperatures above 500 K may be due to emergence of trapping at vacancy clusters, but further experiments that are out of the scope in this work would be necessary to analyze this in detail. Earlier studies[18–20] have reported a 280 ps defect component that has been associated with the gallium monovacancy V_{Ga}. Our values for τ_2 are in good agreement with this assignment, and hence, we conclude that V_{Ga} is the dominant vacancy defect trapping positrons in GaSb.

Figure 3 shows the average lifetime as a function of measurement temperature. Arrows in the figure describe the direction of the temperature scan. The average positron lifetime τ_{ave} corresponds to the center of mass of the lifetime spectrum and is insensitive to the decomposition procedure.

FIG. 2. Lifetimes and intensities as a function of temperature obtained from the two-component model.
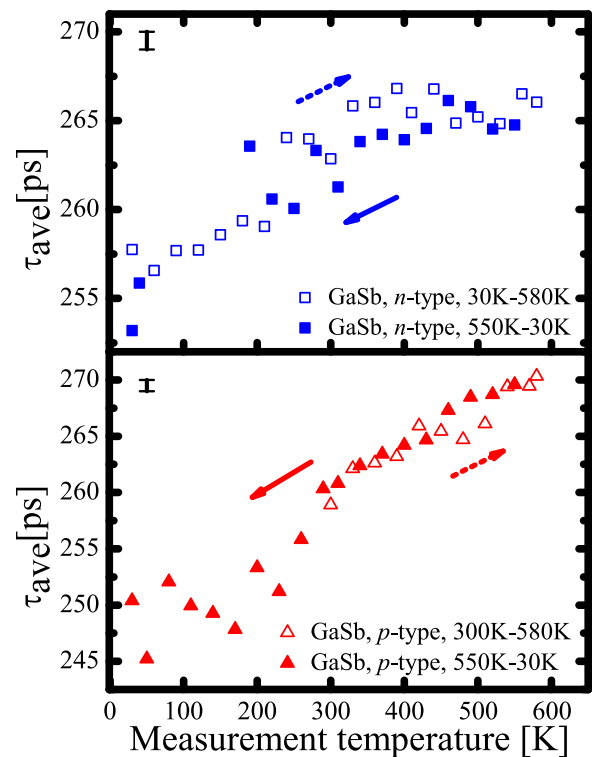
FIG. 3. Positron average lifetime in *p*- and *n*-type GaSb. Statistical errors are marked with error bars drawn at the top left portion of the graphs. Open symbols indicate that the next measurement is done at a higher temperature than the preceding; direction of the temperature change is represented by dashed arrows. Closed symbols indicate that the next measurement is done at a lower temperature than the preceding; direction of the temperature change is represented by full arrows.

The average positron lifetime decreases with decreasing temperature, which is usually a fingerprint of negative non-open volume defects (negative ions) competing in positron trapping with vacancy defects.[15,21] The positron binding energy into a shallow Rydberg-like state is typically around 10–100 meV (Ref. 15) and the de-trapping rate from a Rydberg state increases exponentially with increasing temperature and leads to a rapid decrease of positrons trapping at negative ions above 100–300 K, depending on the binding energy (affected by the dielectric constant and the amount of negative charge). Based on the data in Fig. 3, it is evident that negative ions are important positron trapping centers in both *n*-type and *p*-type GaSb.

IV. DISCUSSION

A. Momentum distributions at different temperatures

Figure 4 shows electron-positron momentum distribution ratios obtained from Doppler broadening measurements at different temperatures. The average positron lifetime is shortest in the *p*-type sample at 30 K. Hence, the electron-positron momentum distribution measured in *p*-type GaSb at 30 K was used as a reference with which the data obtained in other samples and temperatures are normalized. Arrows in the legend indicate the direction of temperature change. The spectra have remarkably little structure compared to typical spectra when vacancies are observed with positrons.[15] The average positron lifetime in the *p*- and *n*-type GaSb increases 20 ps and 15 ps within the temperature range 30–580 K, respectively. This suggests that the annihilation environment should be quite different at 30 K compared to that at 580 K. However, this is not observed in the ratio curves that show that for the most part the annihilation environment resembles that of the reference.

The ratio <1 above 1.2 a.u. in *n*-type GaSb measured at 600 K is due to reduced positron annihilation rate with high momentum Ga 3d electrons. At temperatures above 400 K, the de-trapping rate of positrons from negative ions is higher and trapping to vacancies is increased. While being trapped at V_{Ga} positrons will annihilate more with 4d electrons of the

Sb atom. The momentum distribution of Sb 4d electrons is narrower than that of Ga 3d shell, and hence, a reduction in intensity is seen in the high momentum region of the ratio spectrum. This effect is seen in the *n*-type sample after being cooled down to RT due to the strong trapping of positrons at negative ions. These observations suggest that the negative ion-type positron traps could have higher concentrations than the Ga vacancies.

B. Defect concentrations

The Ga vacancy concentration can be estimated from the average positron lifetime data at RT and above, where the effect of the negative ions is the lowest, using

$$c = \frac{\lambda_B}{N_{at} \cdot \mu} \cdot \frac{\tau_{ave} - \tau_B}{\tau_2 - \tau_{ave}}. \tag{2}$$

Here, a value of 3×10^{15} at. s^{-1} is used for the trapping coefficient[21,22] of negatively charged vacancies at RT. We estimate the positron lifetime in the GaSb lattice to be $\tau_b = 245$ ps based on the low-temperature data in the *p*-type GaSb samples. For the positron lifetime in the Ga vacancy, we use $\tau_2 = 285$ ps (weighted average from our experiments). We obtain $[V_{Ga}] \approx 4 \times 10^{16}$ cm^{-3} in *n*-type GaSb and $[V_{Ga}] \approx 3 \times 10^{16}$ cm^{-3} in *p*-type GaSb.

The concentrations of the negative ion type defects can also be estimated from the positron lifetime data. Assuming that the thermal escape of positrons from the shallow traps is negligible at 30 K, we can solve the kinetic equations[15] without the knowledge of the binding energy to the traps. The trapping coefficient for negative ions is the same as for negative vacancies, and both have $T^{-1/2}$ dependence on temperature. The solution is[23]

$$\kappa_{ion} = \kappa_V \cdot \frac{\tau_2 - \tau_{ave}}{\tau_{ave} - \tau_B}. \tag{3}$$

We estimate the negative ion concentrations to be [ion] $\approx 1 \times 10^{17}$ cm^{-3} in *n*-type GaSb and [ion] $\approx 2 \times 10^{17}$ cm^{-3} in *p*-type GaSb. Hence, the concentration of the negative ions exceeds that of vacancies nearly by an order of a magnitude,
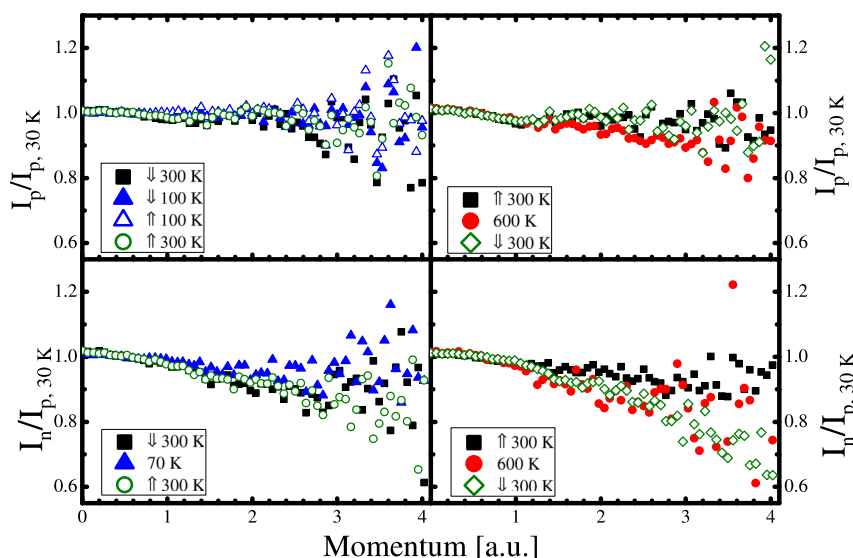

FIG. 4. Momentum distributions at different temperatures. Arrows in the legend indicate the direction of temperature change. Positron lifetime was shortest in *p*-type sample at 30 K. Hence, electron momentum distribution measured for *p*-type GaSb at 30 K was used as a reference.

making them the dominant negatively charged (acceptor) defects in both *n*-type and *p*-type GaSb single crystals.

C. Defect identities and charge states

Virkkala *et al.*[14] calculated the formation energies and charge transition levels for various point defects in GaSb. The GaSb antisite defect has the lowest formation energy of the acceptor-type defects. As the concentrations of the negative ions exceed those of any of the known impurities in both *n*-type and *p*-type samples, we associate them with a native point defect. This defect cannot be of vacancy origin, since it is not observed in the lifetime experiments. Furthermore, the calculations by Virkkala *et al.*[14] suggest that the most likely candidate is a Ga antisite. Hence, in the following, we will focus on the balance between the two acceptor-type defects, namely the V_{Ga} and Ga_{Sb}, observed directly (V_{Ga}) or indirectly (Ga_{Sb}) in our experiments.

According to theoretical calculations,[14] V_{Ga} has three charge transition levels in the band-gap. The (0/1-)-level is below mid-gap close to the valence band maximum at ∼0.1 eV, the (1-/2-)-level is at ∼0.45 eV, i.e., relatively close to mid-gap and the (2-/3-)-level is at ∼0.75 eV, which is close to the conduction band minimum. Ga_{Sb} has two charge transition levels in the band-gap. Both, the (0/1-)- and the (1-/2-)-level are below mid-gap at ∼0.13 eV and at ∼0.27 eV, respectively. The charge transition levels are schematically presented in Fig. 5. The dashed lines are calculated Fermi-level positions at 30 K and 600 K in *p*- and *n*-type GaSb. The arrows in the figure indicate the direction of the movement of the Fermi-level as the temperature is increased.

The positions of the Fermi-level for the *p*- and *n*-type GaSb can be estimated using the available electrical data. The difference between doping concentration and charge carrier concentration in *n*-type GaSb is of the same order of
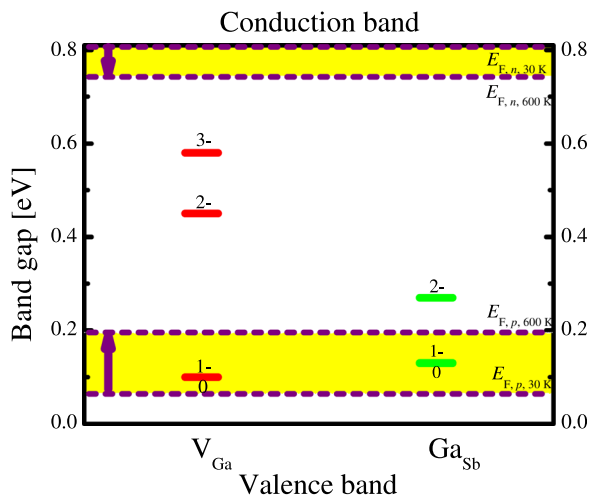
magnitude as the acceptor concentration in undoped *p*-type GaSb ($\sim$1.3 × 10^{17} cm^{-3}). This result is consistent with the temperature behavior of the PAS lifetime measurements. Effective hole and electron masses in GaSb are 0.8 m_e and 0.57 m_e, respectively,[22] where m_e is the mass of the electron. It has to be emphasized, that since some of the values given above are estimates, the results for the Fermi-level position can only be regarded as indicative.

As seen in Fig. 5, V_{Ga} is in the 3- charge state in *n*-type GaSb, i.e., the Fermi-level does not cross the (2-/3-)-level in any measurements. Ga_{Sb} is in the 2- charge state since all the transition levels are below mid-gap. At 30 K most of the positrons annihilate at negative ions, i.e., τ_{ave} in Fig. 3 resembles the assumed vacancy free bulk lifetime. As the temperature is increased, the de-trapping rate from the ions increases and a larger fraction of positrons annihilate at vacancy defects, which is seen as an increase in τ_{ave}. Above 300 K, a plateau is formed since the de-trapping rate from ionic traps is high enough to make vacancy trapping more dominant. As noted above, the Fermi-level positions in Fig. 5 are only indicative, and we believe that the position of the Fermi-level in the *p*-type GaSb is more or less pinned to the (0/1-)-transition level of the Ga_{Sb} at 30 K. Furthermore, the experiments suggests that the (0/1-)-level of Ga_{Sb} is closer to the valence band than the (0/1-)-level of V_{Ga}. Under these conditions, the V_{Ga} could be neutral and the Ga_{Sb} could be in the 1- charge state at 30 K. Hence, the plateau seen in Fig. 3 for the *p*-type GaSb at low temperatures is due to a low trapping ability of neutral V_{Ga}. When the temperature is increased, Fermi-level starts to move towards the mid-gap and the charge state of the V_{Ga} changes from neutral to 1-. This charge transition can be seen in Fig. 5 at ∼200 K, where the plateau ends and the average lifetime starts to increase with increasing temperature. As the temperature is increased further, the average lifetime increases in a linear fashion, suggesting that no additional changes in the charge states of ions or vacancies are seen and that de-trapping from the Ga_{Sb} is not significant The above assignments of charge states are also consistent with the electrical data and the defect (V_{Ga} + Ga_{Sb}) concentrations obtained from positron experiments for *n*-type GaSb: 3 × 4 × 10^{16} cm^{-3} + 2 × 1 × 10^{17} cm^{-3} = 3 × 10^{17} cm^{-3} and in very good agreement with the total estimated acceptor concentration of 1 × 10^{17} cm^{-3}.

V. SUMMARY

In conclusion, we have applied positron annihilation spectroscopy to study native point defects and to identify the origin of *p*-type conductivity in bulk GaSb. Both positron lifetime and Doppler broadening measurements were performed as a function of temperature. The results show that the dominant vacancy defect trapping positrons in bulk GaSb is the gallium monovacancy. The average positron lifetime in both *p*- and *n*-type GaSb indicates that negative ion type defects with no associated open volume compete with the Ga vacancies. Ga antisites in negative charge state are nearly an order of magnitude more abundant compared to that of Ga vacancies and dominate the positron annihilation signal.

FIG. 5. GaSb band gap with charge transition levels of V_{Ga} and Ga_{Sb} after Virkkala *et al.*[14] Fermi-level positions at 30 K and at 600 K in *p*- and *n*-type GaSb are represented with purple dashed lines. Yellow color indicates the area covered by Fermi-level when temperature is increased or decreased. Arrows indicate the direction of Fermi-level movement when temperature is increased.

Hence, we conclude that Ga antisites cause the native *p*-type conductivity in bulk GaSb.

ACKNOWLEDGMENTS

[1]Y. Lu, S. Song, Z. Song, and B. Liu, J. Appl. Phys. **109**, 064503 (2011).

[2]O. Salihoglu, A. Muti, K. Kutluer, T. Tansel, R. Turan, C. Kocabas, and A. Aydinli, J. Appl. Phys. **111**, 074509 (2012).

[3]Z.-X. Yang, F. Wang, N. Han, H. Lin, H.-Y. Cheung, M. Fang, S. Yip, T. Hung, C.-Y. Wong, and J. C. Ho, ACS Appl. Mater. Interfaces **5**, 10946 (2013).

[4]P. Dutta, H. Bhat, and V. Kumar, J. Appl. Phys. **81**, 5821 (1997).

[5]M. Hakala, M. Puska, and R. Nieminen, J. Appl. Phys. **91**, 4988 (2002).

[6]J. J. Mudd, N. J. Kybert, W. M. Linhart, L. Buckle, T. Ashley, P. D. C. King, T. S. Jones, M. J. Ashwin, and T. D. Veal, Appl. Phys. Lett. **103**, 042110 (2013).

[7]M. J. Ashwin, D. Walker, P. A. Thomas, T. S. Jones, and T. D. Veal, J. Appl. Phys. **113**, 033502 (2013).

[8]M. J. Ashwin, R. J. H. Morris, D. Walker, P. A. Thomas, M. G. Dowsett, T. S. Jones, and T. D. Veal, J. Phys. D. Appl. Phys. **46**, 264003 (2013).

[9]M. K. Rajpalke, W. M. Linhart, M. Birkett, K. M. Yu, D. O. Scanlon, J. Buckeridge, T. S. Jones, M. J. Ashwin, and T. D. Veal, Appl. Phys. Lett. **103**, 142106 (2013).

[10]H. Bracht, S. Nicols, W. Walukiewicz, J. P. Silveira, F. Briones, and E. Haller, Nature **408**, 69 (2000).

[11]P. Mooney, J. Appl. Phys. **67**, R1 (1990).

[12]M.-H. Du and S. B. Zhang, Phys. Rev. B **72**, 075210 (2005).

[13]I. Poole, M. Lee, I. Cleverley, A. Peaker, and K. Singer, Appl. Phys. Lett. **57**, 1645 (1990).

[14]V. Virkkala, V. Havu, F. Tuomisto, and M. Puska, Phys. Rev. B **86**, 144101 (2012).

[15]F. Tuomisto and I. Makkonen, Rev. Mod. Phys. **85**, 1583 (2013).

[16]J. Slotte, S. Kilpeläinen, F. Tuomisto, J. Räisänen, and A. N. Larsen, Phys. Rev. B **83**, 235212 (2011).

[17]K. Kuitunen, F. Tuomisto, J. Slotte, and I. Capan, Phys. Rev. B **78**, 033202 (2008).

[18]C. Ling, M. Lui, S. Ma, X. Chen, S. Fung, and C. Beling, Appl. Phys. Lett. **85**, 384 (2004).

[19]W. Hu, Z. Wang, B. Su, Y. Dai, S. Wang, and Y. Zhao, Phys. Lett. A **332**, 286 (2004).

[20]S. Ma, C. Ling, H. Weng, and D. Hang, in *Symposium Z – Progress in Compound Semiconductor Materials III – Electronic and Optoelectronic Applications*, edited by F. D. Auret, I. Buyanova, D. Friedman, M. O. Manasreh, and A. Munkholm (Mater. Res. Soc. Symp. Proc., 2003), Vol. 799.

[21]K. Saarinen, P. Hautojärvi, and C. Corbel, Semicond. Semimetals **51**, 209 (1998).

[22]O. Madelung, in *Data in Science and Technology: Semiconductors* (Springer-Verlag, 1991).

[23]F. Tuomisto, V. Ranki, D. C. Look, and G. C. Farlow, Phys. Rev. B **76**, 165207 (2007).